Published in final edited form as:
J Mol Biol. 2011 June 10; 409(3): 399–414. doi:10.1016/j.jmb.2011.04.004.

Mechanism of Mss116 ATPase reveals functional diversity of DEAD-box proteins

Wenxiang Cao[1], **Maria Magdalena Coman**[1,2], **Steve Ding**[1], **Arnon Henn**[1], **Elizabeth R. Middleton**[3], **Michael J. Bradley**[1], **Elizabeth Rhoades**[1], **David D. Hackney**[4], **Anna Marie Pyle**[1,5], and **Enrique M. De La Cruz**[1,†]

[1]Yale University, Department of Molecular Biophysics & Biochemistry, 260 Whitney Avenue, New Haven, CT 06520, USA

[3]Yale University, Department of Chemistry, New Haven, CT 06520, USA

[4]Department of Biological Sciences, Carnegie Mellon University, 4400 Fifth Avenue, Pittsburgh, PA 15213, USA

[5]The Howard Hughes Medical Institute

Abstract

Mss116 is a *Saccharomyces cerevisiae* mitochondrial DEAD-box RNA helicase protein essential for efficient *in vivo* splicing of all group I and II introns and activation of mRNA translation. Catalysis of intron splicing by Mss116 is coupled to its ATPase activity. Knowledge of the kinetic pathway(s) and biochemical intermediates populated during RNA-stimulated Mss116 ATPase is fundamental for defining how Mss116 ATP utilization is linked to *in vivo* function. We therefore measured the rate and equilibrium constants underlying Mss116 ATP utilization and nucleotide-linked RNA binding. RNA accelerates the Mss116 steady-state ATPase ~7-fold by promoting rate-limiting ATP hydrolysis, such that P_i release becomes (partially) rate-limiting. RNA binding displays strong thermodynamic coupling to the chemical states of the Mss116-bound nucleotide such that Mss116 with bound ADP-P_i binds RNA more strongly than with bound ADP or in the absence of nucleotide. The predominant biochemical intermediate populated during *in vivo* steady-state cycling is the strong RNA binding, Mss116-ADP-P_i state. Strong RNA binding allows Mss116 to fulfill its biological role in stabilization of group II intron folding intermediates. ATPase cycling allows for transient population of the weak RNA binding, ADP state of Mss116 and linked dissociation from RNA, which is required for the final stages of intron folding. In cases where Mss116 functions as a helicase, the data collectively favor a model in which ATP hydrolysis promotes a weak-to-strong RNA binding transition that disrupts stable RNA duplexes. The subsequent strong-to-weak RNA binding transition associated with P_i release dissociates RNA-Mss116 complexes, regenerating free Mss116.

Keywords

RNA helicase; ATPase cycle; kinetics; fluorescence correlation spectroscopy (FCS)

[†]Address correspondence to: Enrique M. De La Cruz, Yale University, Department of Molecular Biophysics & Biochemistry, P.O. Box 208114, New Haven, CT, 06520-8114. Tel. (203) 432-5424; Fax. (203) 432-1296; enrique.delacruz@yale.edu..
[2]Current address: Yale University, Department of Medicine Laboratory, New Haven, CT 06520, USA

Introduction

DEAD-box proteins are a family of RNA-stimulated ATPase enzymes that couple ATP utilization to local conformational rearrangement of RNA [1; 2; 3; 4; 5; 6] at all levels of RNA metabolism, including transcription and replication, protein translation, pre-mRNA splicing and editing, ribosome biogenesis, RNA export to the cytoplasm, and RNA degradation [7; 8; 9; 10; 11; 12; 13]. Mss116 is an essential *Saccharomyces cerevisiae* mitochondrial DEAD-box protein that is required for the splicing of all group I and II introns [14; 15; 16; 17; 18; 19] and for active mRNA translation [14; 17; 20]. The ability of Mss116 to stimulate group I and II intron splicing correlates with RNA-unwinding activity [20], although efficient helix unwinding is neither essential [15] nor sufficient [18] for splicing activity[14; 15; 16; 21; 22]. These data indicate that Mss116 has multiple mechanistic roles during the course of intron splicing and that it may have different functions on different types of RNA substrates [22; 23].

Quantitative determination of the discrete steps associated with RNA-stimulated Mss116 ATPase activity is essential for understanding its biological role in stimulating the efficient splicing of all group I and II introns and in activating mitochondrial mRNA translation. However, mechanistic details regarding Mss116 ATPase enzymology is lacking, including the kinetic and equilibrium constants defining ATP utilization, the biochemical intermediates populated during catalytic cycling, and the coupling between ATP consumption and RNA interactions along the reaction pathway.

Here, we present a quantitative kinetic and equilibrium analysis of the RNA-stimulated ATPase and nucleotide-linked RNA binding activities of Mss116. Bound RNA stimulates the Mss116 ATPase by promoting ATP hydrolysis. RNA binding is nucleotide-dependent, yielding “weak” and “strong” RNA binding states. The RNA binding affinity of Mss116 progressively increases with ATP binding and subsequent hydrolysis, and then weakens by more than two orders of magnitude after phosphate is released. This knowledge advances our understanding of the molecular mechanism of coupling between Mss116 ATP utilization and RNA conformational rearrangement, and permits the development of predictive ATPase-dependent models of Mss116 catalyzed group I and II intron splicing and mRNA translation.

Results

Steady-state ATPase activity of Mss116

RNA enhances the maximal Mss116 steady-state ATPase activity (k_{cat}) ~7-fold from 0.26 $s^{-1}Mss116^{-1}$ to 1.5-1.8 s^{-1} $Mss116^{-1}$ (Fig. 1, Table 1), within the range of 0.17-3.5 $s^{-1}Mss116^{-1}$ measured for full-length and truncated Mss116 using different assays with various RNA substrates under slightly different temperature and buffer conditions [16; 21; 24]. The ATPase of Mss116 alone is not due to contaminating RNA in our preparation, as identical rates are obtained in the presence of RNAse A (Figure 1) The apparent Michaelis constant for RNA ($K_{M,RNA}$) in the presence of saturating ATP (10 mM) is ~200 nM (Fig. 1B, Table 1). The Michaelis constant for ATP ($K_{M,ATP}$) in the presence of near saturating RNA (2 μM) is ~250 μM (Fig. 1C, Table 1), also within the range of values (88 – 633 μM) reported for full length Mss116 with various RNA substrates [16; 18]. The [RNA]-dependence of the steady-state ATPase measured with 2 μM Mss116 (>>$K_{M,RNA}$) yields an ATPase activation stoichiometry of 0.9 RNA per Mss116 (Fig. 1D; Table 1).

Minimal Mss116 ATPase cycle

The minimal reaction scheme of discrete reaction steps (Scheme 1) was used to model the RNA-activated ATPase of Mss116 and analyze experimental data acquired from the transient kinetic and equilibrium binding experiments presented in subsequent sections. In Scheme 1, Mss116 helicase exists in free (*H*) and RNA-bound (*RH*) forms either with or without bound adenine nucleotides *T* (ATP) or *D* (ADP); P_i is inorganic phosphate. We assume product release is sequential with P_i dissociation preceding ADP dissociation, include two stable Mss116-ADP states based on the data presented forthcoming, and for simplicity do not include non-specific collision complexes that precede stable complex formation [25; 26]. It is also likely that ATP hydrolysis is limited by a conformational change preceding chemical cleavage of the gamma phosphate bond of ATP [3; 4]; for simplicity, we treat this activated ATP-bound state and the hydrolysis reaction as a single biochemical species since they are kinetically equivalent. We emphasize that Scheme 1 is a *minimal* ATPase cycle scheme, analogous to that used to model other lattice-activated ATPases (e.g. myosin [27]) and that a more complex Scheme with additional intermediates could potentially apply.

Nucleotide binding to Mss116

ATP and ADP binding to Mss116 and Mss116-RNA was measured from the fluorescence enhancement associated with Förster resonance energy transfer from Mss116 to bound mant-nucleotides [3; 28; 29]. Mss116 possesses five tyrosine residues between the Walker A and Walker B sequence motifs of the nucleotide binding site and no tryptophan residues; energy transfer presumably occurs from Mss116 tyrosines to mant.

Time courses of fluorescence enhancement after mixing mantATP or mantADP with Mss116 or Mss116-RNA are multiphasic and best fitted to a four exponential function (Figs. 2A, 2B, 3A and 3B). The two fast relaxations (λ_1 and λ_2) depend on the [mant-nucleotide], while the two slow relaxations (λ_3 = 1-4 s^{-1} and λ_4 = 0.1-0.4 s^{-1}) are independent over the range examined (Figs. 2C, 2D, 3C and 3D) and are similar with mantATP and mantADP, both with and without RNA. We limit our analysis and discussion to the two fast, [mant-nucleotide]-dependent phases. We do not include analysis of the slow components because they are either too slow to be ATPase on-pathway reactions (i.e. $\lambda < k_{cat}$) and/or they have small and variable amplitudes that preclude reliable quantitative analysis. Future studies are needed to identify the nature of the biochemical transitions associated with these spectroscopic changes, though they may reflect off-pathway isomerization reactions [25], minor protein or nucleotide impurities and/or mant isoform-specific interaction kinetics [30].

We interpret that the fastest observed mantATP phase (λ_{1T}) as binding because the [mantATP]-dependence is approximately linear [3; 25] (Figs 2B and 2C). Mss116 possesses ATPase activity (Fig. 1), even in the absence of RNA, so the second relaxation (λ_{2T}) after ATP binding includes contributions from binding, hydrolysis, and subsequent product release [3]. We therefore globally fitted the [mantATP]-dependence of the two observed rate constants using the following equations that account for contributions from ATP binding, hydrolysis and phosphate release [3]:

$$\lambda_{1T,2T}=\frac{1}{2}\left(k_{+RT}[T]+k_{-RT}+\lambda_{2T,\infty} \pm \sqrt{\left(k_{+RT}[T]+k_{-RT}+\lambda_{2T,\infty}\right)^2-4\left(k_{+RT}[T]\lambda_{2T,\infty}+k_{-RT}\lambda_{2T,0}\right)}\right) \quad (1),$$

with

$$\lambda_{2T,\infty} = k_{+RH} + k_{-RH} + k_{-RPi} \quad (2),$$

and

$$\lambda_{2T,0} = \frac{k_{-RT}k_{-RH} + k_{-RT}k_{-RPi} + k_{+RH}k_{-RPi}}{k_{-RT}} \quad (3),$$

where the term $\lambda_{2T,\infty}$ is the maximum value of λ_{2T} at saturating ATP concentration and the term $\lambda_{2T,0}$ is approximately equal to the initial value of λ_{2T} (i.e. extrapolated to zero ATP)[3]. The values of $\lambda_{2T,\infty}$ and $\lambda_{2T,0}$ together with isotopic exchange and transient P_i release data are used to obtain the ATP hydrolysis, resynthesis and P_i release rate constants [3] (presented forthcoming). These expressions also apply to no RNA conditions since Mss116 possesses an intrinsic ATPase activity.

RNA accelerates ATP binding to Mss116 by almost an order of magnitude (k_{+RT} = 2.1 μM^{-1} s^{-1} and k_{+T} = 0.33 μM^{-1} s^{-1}) and slows ATP dissociation ~2-fold (k_{-RT} = 35 s^{-1} and k_{-T} = 66 s^{-1}), thereby yielding overall tighter ATP binding constant ($K = k_{-}/k_{+}$; K_{RT} ~ 17 μM and K_T ~200 μM). The amplitude of fluorescence change yields a comparable value of 125 μM for K_T (Fig. 2E; Table 1).

MantADP binding also displays two fast, concentration-dependent phases (λ_{1T} and λ_{2D}). The observed relaxations in this case have different meaning than with mantATP, since hydrolysis and product release reactions are absent. The [mantADP]-dependence of λ_{1D} and λ_{2D} (Figs. 3C and 3D) is modeled as a consecutive two-step binding reaction (ignoring collision complex formation [26]) and globally fitted to the following quadratic equations for reversible two-step binding[3; 25]:

$$\lambda_{1D,2D} = \frac{1}{2}\left(k_{+1RD}[D] + k_{-1RD} + k_{+2RD} + k_{-2RD} \pm \sqrt{(k_{+1RD}[D] + k_{-1RD} + k_{+2RD} + k_{-2RD})^2 - 4(k_{-2RD}k_{-1RD} + k_{-2RD}k_{+1RD}[D] + k_{+2RD}k_{+1RD}[D])}\right)$$

(4),

to obtain the fundamental ADP binding rate constants (Table 1).

The overall mantADP binding affinity for Mss116 ($K_{D,overall}$) and for Mss116-RNA ($K_{RD,overall}$) estimated from the total amplitude of the fluorescence change are ~ 43 μM (Fig. 3E) and ~92 μM, respectively (data not shown; Table 1), comparable to the predicted values of ~25 μM and ~70 μM (Table 1) calculated from the individual step-wise ADP equilibrium binding constants [3; 25].

Time courses of irreversible mantADP release from Mss116 and Mss116-RNA also display multiple phases (Fig. 4), in accord with the time courses of association (Figs. 2 and 3). The two fast relaxations ($\lambda_{diss,1}$ and $\lambda_{diss,2}$) with Mss116 alone are ~69 s^{-1} and ~13 s^{-1}, which correlate with the values of ~64 s^{-1} and ~9 s^{-1} predicted from mantADP association using the following expression [3; 25]:

$$\lambda_{\text{diss1,diss2}}=\frac{1}{2}\left(k_{-1D}+k_{+2D}+k_{-2D}\pm\sqrt{(k_{-1D}+k_{+2D}+k_{-2D})^2-4k_{-1D}k_{-2D}}\right) \quad (5),$$

indicating internal consistency of association and dissociation data. Similarly, the fast relaxations with Mss116-RNA are ~194 s^{-1} and ~17 s^{-1}, comparable to the predicted values of ~172 s^{-1} and ~20 s^{-1} (Table 1).

Oxygen isotopic exchange

^{18}O isotopic exchange [31; 32] was used to measure reversibility of ATP hydrolysis by Mss116 and Mss116-RNA during steady-state cycling. The reversibility of ATP hydrolysis is indicated by the partition coefficient P_c, which reflects the probability of ATP resynthesis from bound ADP and P_i (k_{-H} or k_{-RH}) relative to P_i release (k_{-Pi} or k_{-RPi}) and is given by [31; 32]:

$$P_c\,(-RNA)=\frac{k_{-H}}{k_{-H}+k_{-Pi}} \quad \text{or} \quad P_c\,(+RNA)=\frac{k_{-RH}}{k_{-RH}+k_{-RPi}} \quad (6).$$

The P_c values for reversibility of ATP hydrolysis by Mss116 and Mss116-RNA are 0.147 and 0.088, respectively (Table 1). The low P_c values indicate a small number of hydrolysis reversals during steady-state ATPase cycling. The number of reversals in the presence of RNA, however, is smaller than in its absence.

Phosphate release

Transient P_i from Mss116 or Mss116-RNA upon addition of ATP was measured with the fluorescently labeled mutant of phosphate binding protein (MDCC–P_iBP). Time courses of inorganic phosphate (P_i) release from Mss116-RNA display a lag phase followed by a linear regime (Fig. 5A). The observed lag phase arises from formation of at least one biochemical intermediate(s) prior to P_i release on the first cycle pass (i.e. approach to steady-state turnover) with a rate constant comparable or slower than that of P_i release [3]. That is, two transitions in series with comparable rate constants must exist. The prominent lag and lack of a P_i release burst phase [25] indicate that ADP release is not rate-limiting during steady-state ATPase turnover (i.e. k_{cat}), and that either hydrolysis, P_i release or both limit Mss116 cycling in the presence of RNA.

Scheme 1 predicts that time courses of irreversible P_i release (fulfilled with presence of phosphate binding protein, P_iBP) follow an exponential decay (λ_{lag}) preceding a linked linear regime (C) given by [3]:

$$[P_i]=C\left(\frac{1}{\lambda_{lag}}\left(e^{-\lambda_{lag}t}-1\right)+t\right) \quad (7).$$

The observed lag phase rate constant (λ_{lag}; equivalent to λ_{2T} in mantATP association presented earlier [3]) depends hyperbolically on [ATP] (Fig. 5B), displaying a lower limit ($\lambda_{lag,0}$) of ~3 s^{-1} and approaches a maximum ($\lambda_{lag,\infty}$) of ~12 s^{-1} at saturating ATP that is proportional to the sum of ATP hydrolysis (k_{+RH}) or more likely a conformational change preceding rapid ATP hydrolysis [3] (these are kinetically equivalent), ATP resynthesis (k_{-RH}) and P_i release (k_{-RPi}) rate constants (Eq. 2; Ref. [3]). The values of $\lambda_{lag,\infty}$ and $\lambda_{lag,0}$ compare to the values of $\lambda_{2T,0}$ (~4 s^{-1}) and $\lambda_{2T,\infty}$ (~20 s^{-1}) obtained with mantATP (Fig. 2D, Table

1) as predicted from Scheme 1. The [ATP] at which λ_{lag} reaches half maximal value ($K_{0.5}$ ~80 μM) approximates the ATP binding constant of Mss116-RNA [3]:

$$K_{0.5}=K_{RT}=\frac{k_{-RT}}{k_{+RT}} \quad (8).$$

The value of K_{RT} for mantATP (K_{RT} ~ 16 μM, Table 1) is ~5 times tighter than that of ATP, presumably due to favorable interactions with the mant moiety [3; 28; 29]. The slope of the linear phase reflects steady-state ATP turnover and thus depends hyperbolically on [ATP] (Fig. 5C), yielding $K_{M,ATP}$ of ~300 μM, comparable to the value of ~250 μM measured with the NADH-coupled assay (Table 1).

The experimental values of P_c from ^{18}O exchange, $\lambda_{lag,\infty}$ and $\lambda_{lag,0}$ of the P_i release lag phase, and k_{-RT} and k_{-T} from mantATP binding permit determination [3] of the ATP hydrolysis (k_{+RH} = 9.7 s^{-1} and k_{+H} = 1.1 s^{-1}), ATP resynthesis (k_{-1RH} = 0.23 s^{-1} and k_{-H} = 1.8 s^{-1}), and P_i release (k_{-RPi} = 2.4 s^{-1} and k_{-Pi} = 10.4 s^{-1}) fundamental rate constants. The rate constants differ slightly with mantATP (calculated using $\lambda_{2T,0}$ and $\lambda_{2T,\infty}$ rather than $\lambda_{lag,\infty}$ and $\lambda_{lag,0}$ from P_i release): k_{+RH} = 16.5 s^{-1}, k_{-RH} = 0.26 s^{-1} and k_{-RPi} = 2.7 s^{-1}, indicating that mant labeling accelerates ATP hydrolysis ~2-fold without affecting ATP resynthesis or P_i release.

Since mantATP binds more tightly than ATP, the values of k_{-RT} and k_{-T} used for analysis could introduce uncertainty. To estimate the possible deviation, we evaluated how the values of k_{-RT} and k_{-T} influence the rate constant output. When the values of k_{-RT} and k_{-T} are varied from 20 to 200 s^{-1}, the results deviate by ±0.2-0.6 s^{-1} for ATP hydrolysis, ±0.03-0.05 s^{-1} for ATP resynthesis, and ±0.1-0.6 s^{-1} for phosphate release. Therefore, uncertainties in the ATP dissociation rate constants minimally affect the ATP hydrolysis, ATP resynthesis and P_i release rate constant values.

Equilibrium binding of Mss116 and RNA by FCS

Equilibrium binding of Mss116 and Mss116-ADP to RNA measured by anisotropy suggested the possibility of light scattering at high protein concentrations, possibly caused by protein aggregation (see below). Therefore equilibrium binding of Mss116 and Mss116-ADP to RNA was measured by FCS to directly visualize solution mobility of the complexes. The observed decay time of the fluorescence autocorrelation of RNA increases with [Mss116] (Fig. 6A). Global fitting of the time courses to a two-component autocorrelation function (Eq. 11) [33; 34; 35] yields diffusion times (Table 1) for free RNA (τ_{RNA} = 0.27 ms and 0.26 ms in the presence of 10 mM ADP) and Mss116-RNA ($\tau_{complex}$ = 0.69 ms) or Mss116-ADP-RNA ($\tau_{complex,ADP}$ = 0.56 ms). The [Mss116]-dependence of the bound RNA fraction (Eq. 12) yields overall RNA binding affinities of 117 nM for Mss116 and 775 nM for Mss116-ADP (Table 1). Comparable affinities (122 nM for Mss116 and 848 nM for Mss116-ADP) are obtained (Eq. 14) from fitting the [Mss116]-dependence of the average diffusion time ($\tau_{average}$) from a single component autocorrelation function (Eq. 11) [33; 34; 35]. Detailed balance yields binding affinities of ~47 nM for Mss116-ATP and 2 nM for Mss116-ADP-P_i (Table 1). The overall affinity of Mss116-ADP, accounting for both ADP-bound states, calculated from detailed balance is ~340 nM (Table 1), about a factor of two with the value measured by FCS. The diffusion time of Alexa488-labeled Mss116 is 0.52 ms (Table 1), slightly shorter than those of the Mss116-RNA complex as expected.

We note that autocorrelation time courses deviate between consecutive measurements, such that they display a lower total number of molecules (N) and longer diffusion time (τ) with [Mss116] > 200 nM and [Mss116-ADP] > 500 nM and low (20 nM) RNA, characteristic of

slow protein oligomerization. Oligomerization is observed only at [Mss116] >> [RNA] and is weakened by ADP. While self-association may play a role in Mss116 activity, the characterization is beyond the scope of the current work and we reserve investigation for future work. Throughout the current study, Mss116 was maintained at concentrations where oligomerization did not occur or with [RNA] > [Mss116].

Kinetic simulations and modeling

Simulated time courses of steady-state phosphate release from Mss116-RNA using Scheme 1 and the reaction constants obtained in this work (Table 1) account for the experimental time courses of transient and steady-state P_i release (dotted line in Fig. 5A), demonstrating that the rate constants and equilibrium constants obtained from the different measurements and assays are consistent with the observed Mss116-RNS ATPase cycling behavior.

Furthermore, the macroscopic steady-state parameters (k_{cat} and K_M) predicted from the rate and equilibrium constants agree well with the experimentally determined values (Table 1), further strengthening the validity of the ATPase cycle model (Scheme 1) and experimental constants (Table 1). In the absence of RNA, Mss116 has low but detectable ATPase activity with a k_{cat} value of ~0.3 $s^{-1}Mss116^{-1}$ (Fig. 1A, Table 1). The k_{cat} value predicted (Eq. A29, Supplementary material) from the rate and equilibrium constants derived in this study (Table 1) is 0.8 $s^{-1}Mss116^{-1}$. The three-fold difference and higher predicted value is likely a consequence of using mantATP binding parameters. If we assume that in the absence of RNA, ATP hydrolysis occurs 2-fold more slowly than mantATP, as was observed with Mss116-RNA (Table 1), the predicted k_{cat} value with ATP is 0.4 $s^{-1}Mss116^{-1}$, significantly closer to the experimentally observed value. The predicted k_{cat} value in the presence of RNA (Eq. A23, Supplementary material) is 1.7 s^{-1} $Mss116^{-1}$, similar to the experimental value of 1.5-1.8 $s^{-1}Mss116^{-1}$ (Fig. 1B, Table1). In these and forthcoming calculations of $K_{M,ATP}$ and $K_{M,RNA}$, we use the overall ADP binding and dissociation rate constants at steady state.

The $K_{M,RNA}$ and $K_{M,ATP}$ values predicted from Eq. A21 (Supplementary material) and Eq. 42 in the Appendix of Ref. [3], respectively, however, differ from those measured experimentally; ~3-fold for $K_{M,RNA}$ and ~10-fold for $K_{M,ATP}$ (Table 1). While this may result from experimental uncertainty, the large discrepancy with $K_{M,ATP}$ could reflect weaker ATP binding during steady-state cycling than to the initial nucleotide-free complex, raising the possibility that they adopt somewhat different structural states. Similarly, the initial RNA structure may differ from the average during cycling.

Distribution of populated biochemical intermediates

Knowledge of the ATPase cycle rate and equilibrium permits evaluation of the transiently populated biochemical intermediates and their distribution during steady-state ATPase cycling under *in vitro* (10 mM ATP, 0.030 mM ADP) and *in vivo* conditions (1.2 mM ATP, 0.11 mM ADP and 2.7 mM Pi with 110 mM glucose in yeast *Saccharomyces cerevisiae* mitochondria [36]) conditions (Fig. 7). During *in vivo* and *in vitro* steady state cycling, the majority of Mss116-RNA complex (70%) exists as the ADP-P_i state; smaller fractions (10-20%) populate the ATP- or ADP-bound states, and essentially none exists in the nucleotide-free form. In contrast, in the absence of RNA most Mss116 populates the ATP- (*in* vivo 46%, *in vitro* 80%) and ADP-bound states (*in* vivo 42%, *in vitro* 11%); small fractions of the total are nucleotide-free (8% *in vivo*, 2% *in vitro*) or with bound ADP-P_i (4% *in* vivo, 7% *in vitro*).

RNA duplex unwinding by Mss116

RNA duplex unwinding by Mss116 was measured under single turnover conditions (i.e. [*Mss116*] >> [*dsRNA*]) using a fluorescence anisotropy-based duplex RNA strand

displacement assay [4]. This duplex RNA was used as an unwinding substrate for the DEAD-box protein, DbpA, and consists of a fluorescently-labeled 8-mer RNA single strand annealed to a 32-mer mother strand fragment [4]. Time courses of 8-bp RNA strand displacement by saturating [Mss116] and ATP are biphasic (Fig. 8) with a fast phase (k_{sd} (+ATP)) of 2.1 s^{-1} comprising ~70% of the total amplitude, followed by a second, slower phase of ~0.1 s^{-1} (Table 1). The fraction of duplex unwound depends on the [Mss116], [RNA] and duplex binding affinity [4]. In the absence of ATP, a very small portion of the 8-bp RNA duplex is displaced by saturating Mss116 with a rate constant (k_{sd} (−ATP)) of 0.1-0.2 s^{-1} (Fig. 8), suggesting the slow phase in the presence of ATP represents an ATP-independent event.

We estimate that a minimum of ~1.4 ATP molecules are used per strand displacement event by converting the single-turnover strand displacement rate constant (k_{sd}) to an average strand displacement rate in the absence of reannealing (i.e. irreversible strand displacement):

$$\langle Strand \quad displacement \quad rate \rangle = k_{sd}\left(1 - e^{-1}\right)[duplex \quad RNA] \tag{9},$$

and comparing to the steady-state ATP utilization rate for the same [duplex RNA]. This calculation assumes strand displacement is 100% efficient, so represents a minimum ATP utilization value. Reannealing of a (partially) unwound strand will lead to futile ATP cycling and increase the number of ATP's hydrolyzed per productive event. We also note that these measurements were made under conditions where Mss116 oligomerization was observed by FCS, so the Mss116-RNA stoichiometry during unwinding is uncertain and requires further investigation.

Discussion

RNA-activation of Mss116 ATPase

RNA enhances the slow intrinsic ATPase activity of Mss116 ~7-fold by accelerating rate-limiting ATP hydrolysis (Table 1). RNA also slows ATP resynthesis from bound ADP and P_i hydrolysis products ~8 fold (Table 1), yielding a >70 times more favorable ATP hydrolysis equilibrium constant when bound to RNA (Table 1). Therefore, RNA-dependent acceleration of Mss116 ATP utilization arises from both kinetic and thermodynamic effects. RNA also slows P_i release from Mss116, such that it is the slowest transition in the RNA-activated ATPase cycle pathway, and becomes partially rate-limiting with ATP hydrolysis, which is only ~4-fold faster (Table 1). Stabilization of the "closed" helicase core interdomain cleft conformation [3; 4; 37; 38; 39] with RNA binding could potentially account for slower P_i release.

RNA-Nucleotide Binding Linkage

The RNA and nucleotide binding sites of Mss116 are chemically linked. ADP weakens RNA binding affinity and vice-versa (Table 1). In contrast, ATP favors RNA binding; there is a corresponding increase in ATP affinity when RNA is bound (Table 1) [3; 4; 37; 38].

There is a step-wise increase in RNA binding affinity as Mss116 progresses through its ATPase cycle ($HR \rightarrow HRT \rightarrow HRDP_i$), then a dramatic weakening by more than two orders of magnitude after P_i release (*HRD*); nucleotide-free Mss116 binds RNA weakly (K_d ~ 120 nM); Mss116-ATP binds more strongly (K_d ~50 nM); Mss116-ADP-P_i binds with highest affinity (K_d ~ 2nM) and Mss116-ADP binds with the lowest affinity of all chemical states (K_d ~ 340 nM). Although the absolute affinities span a broad range, we classify Mss116-ADP-P_i as a "strong" RNA binding state, and nucleotide-free and Mss116-ADP states as

"weak" RNA binding states. Mss116-ATP binds with an "intermediate" affinity – more tightly than nucleotide-free and Mss116-ADP, but considerably weaker than Mss116-ADP-P_i.

ATPase-coupled conformational rearrangement of RNA

It has been proposed that RNA duplex destabilization by the DEAD-box protein, DbpA, coincides with the "weak-to-strong transition" (ATP hydrolysis [3; 4]) and strand dissociation occurs as a diffusive process from the strongly-bound ADP-P_i intermediate [4]. ATP and RNA binding are weakly coupled in DbpA, so ATP binding *per se* does not promote significant displacement of an 8-mer RNA duplex strand [4]. The large free energy change of ATP binding promotes a conformational change of the DbpA-RNA complex [3; 4; 37; 38].

The coupling, albeit weak, between ATP and RNA binding observed for Mss116 (Table 1) raises the possibility that ATP binding can promote local reorganization and/or partial unwinding of bound duplex RNA, given that this transition is linked to stronger RNA binding. RNA duplex unwinding with ATP binding (i.e. hydrolysis independent) has been reported for Cyt19 [6] and DED1 [5], suggesting that ATP and RNA binding may be strongly coupled in these DEAD-box protein family members. However, AMPPNP-state of DbpA and other DEAD-box proteins bind RNA strongly without any detectable strand displacement, indicating that additional reactions contribute to productive duplex RNA strand displacement. Local, partial reorganization, however, could conceivably displace short (<8 bp) duplex fragments [40].

Implications for intron splicing activity

ATP utilization cycles Mss116 vectorially through a series of nucleotide-linked structural states with varying RNA affinities. ATPase cycling maintains Mss116 in predominantly the strong RNA binding and duplex RNA destabilizing, ADP-P_i conformation during steady-state, both under *in vitro* and *in vivo* conditions, but also allows it to transiently populate states that bind RNA weakly. These nucleotide-dependent oscillations in Mss116-RNA binding activity are suited for facilitation of intron splicing and are consistent with recent studies investigating Mss116-catalyzed group II intron folding [23; 41]- Mss116 with bound ADP-P_i strongly binds and reorganizes RNA structure; subsequent P_i release promotes weak RNA binding, thereby dissociating the complex, allowing intron self-splicing and regenerating free Mss116 for additional rounds of catalysis.

Mss116 stimulated intron splicing is extremely slow, displaying a second order rate constant of $< 0.001\ nM^{-1}\ s^{-1}$, considerably slower than the unwinding and strand displacement rates of various duplex RNAs [15; 16; 20; 21; 22; 24; 42] as well as the short 8 bp duplex evaluated in this study, which consumes ~1-2 ATP per displacement event. This large difference between rate constants for splicing and duplex unwinding suggests that multiple ATP molecules are hydrolyzed per productive splicing event. Multiple ATP hydrolysis events could arise if catalysis of intron splicing requires large-scale reorganization of the RNA (potentially occurring through mechanical remodeling of many RNA segments), or it may arise from futile cycling of Mss116 prior to its release during the final stage of intron assembly.

Functional diversity DEAD-box protein function and ATPase

Numerous advances concerning the molecular mechanism of DEAD-box protein helicase and RNA chaperone activity have been made in recent years (reviewed in Refs. [1; 2; 43]). Large bodies of these works have focused on the structures, unwinding and chaperone activities, and biological functions of this family of enzymes. Although the linkage between nucleotide and RNA interactions in DEAD-box proteins is established [3; 4; 5; 6; 37; 38; 44; 45; 46], considerably less knowledge of the ATPase cycle

enzymology, particularly the significance and role of transiently populated ATPase cycle biochemical intermediates, is available. To the best of our knowledge, the ATPase cycles of only two DEAD-box proteins, DbpA [3] and Mss116 (this study), have been characterized completely at the kinetic and thermodynamic level. Despite the limited sampling, evidence for DEAD-box protein ATPase cycle adaptations contributing to specific biological functions is beginning to emerge.

The reaction pathway for the ATPase cycle appears to be conserved for DbpA and Mss116 in that the kinetic intermediates and the order in which these intermediates are populated are similar. The ATPase cycles of DbpA and Mss116 are both partially limited by ATP hydrolysis and subsequent P_i release, with P_i release being the slower of the two transitions. As a result, the predominantly populated biochemical intermediate during steady-state cycling under *in vitro* conditions is the ADP-P_i state for both DbpA and Mss116.

The distribution of populated intermediates under *in vivo* conditions differs between DbpA and Mss116. DbpA exists predominantly in the ADP-form *in vivo* nucleotide concentrations, whereas Mss116 largely populates the ADP.P_i state. DbpA has been suggested to promote conformational rearrangement of hairpin 92 of 23S ribosomal RNA [47], thereby contributing to ribosome biogenesis and/or assembly [48]. It has been suggested that population of the weak(er) RNA binding, ADP nucleotide state of DbpA allows for transfer unwound rRNA product to ribosomal proteins and/or assembly cofactors *in vivo* [3].

In contrast, Mss116 largely populates the strong RNA binding, ADP.P_i conformation under *in vivo* conditions. It is likely that strong RNA binding allows Mss116 to fulfill its biological role in stimulating intron splicing, as reported for facilitated group II intron folding [23]. ATPase cycling allows for transient population of the (very) weak RNA binding, ADP state of Mss116 and linked dissociation from RNA [23], at which point the unconstrained introns undergo self-splicing.

Materials and Methods

Reagents

All reagents were the highest purity commercially available and came from Sigma, unless otherwise noted. Solutions were prepared using MilliQ dispensed water that had been treated for 8 hours with diethyl pyrocarbonate at 1 mL per liter, then autoclaved. RNase activity was undetectable in all reagents, buffers, and protein preparations. Mixed 2′- and 3′-*o*-mant (*N*-methylanthraniloyl) nucleotides were purchased from Invitrogen. A molar equivalent of $MgCl_2$ was added to nucleotides immediately before use.

Protein

The Mss116 protein used in this study is a truncated construct with the C-terminal basic tail (residues 598-664 of full length Mss116) and N-terminus (residues 1-72, including the mitochondrial signal sequence [24]) removed. The rationale for use of this construct has been carefully considered. Full-length Mss116 was partially insoluble at concentrations needed for the biochemical studies presented in this study, presumably due to largely unstructured N- and C-termini extensions, as suggested by secondary structure prediction algorithms (Jpred 3 secondary structure prediction server; http://www.compbio.dundee.ac.uk/jpred [49]). Limited proteolysis yielded a soluble Mss116 protein core region (Ser73 - Tyr597) that retains RNA-stimulated ATPase activity (presented forthcoming) and robust catalysis of model group II intron splicing (data not shown). This construct is slightly larger than the available atomic resolution structure (Ser88 -Asp596 [50]).

Truncated Mss116 was cloned into pETSUMO (Invitrogen) and overexpressed in Rosetta 2(DE3) cells (Novagen). Overnight cultures were freshly diluted 1:100 into LB media and grown at 37 °C to an OD_{600} of 0.5–0.6. The cultures were allowed to grow for 30 min. at 16 °C, induced with 0.25 mM IPTG, and incubated for an additional 20 h. Cells were harvested by centrifugation at 6000 x *g* for 10 min., resuspended in lysis buffer (25 mM HEPES-KOH, 500 mM KCl, 10 % glycerol, 5 mM β-mercaptoethanol, 10 mM imidazole, pH 8.0) and lysed by three passes through a MicroFluidizer at 15,000 psi. The lysate was cleared by centrifugation at 15,000 x *g* for 30 min., and the supernatant was allowed to batch-bind Ni-NTA beads (Qiagen) for 1 h. Beads were washed with 10 resin volumes of lysis buffer followed by 10 column volumes of wash buffer (lysis buffer with 20 mM imidazole). Bound Mss116 was eluted from beads with 4 column volumes of elution buffer (lysis buffer with 160 mM imidazole), the eluate was diluted three-fold using storage buffer (lysis buffer without imidazole) and treated with GST-tagged SUMO protease (construct generously provided by Mark Hochstrasser (Yale University)) and purified to remove the SUMO tag. After proteolysis, the solution was passed over tandem GST-Ni^{2+} columns to remove SUMO protease and cleaved SUMO tag. Mss116 protein was concentrated using an Amicon Ultra 50 kD cut-off centrifugal filter (Millipore) and gel-filtered over Superdex 200 equilibrated in storage buffer.

RNA

Measurements were made with the following folded [3] 28-mer RNA substrate (Dharmacon, Thermo Fisher Scientific, Inc.): GCCUCGCUGCCCUUCGGGGCAGCGAGGC. RNA structure prediction by RNAstructure (by Mathews lab, http://rna.urmc.rochester.edu/RNAstructure.html) indicates that this sequence adopts a blunt end 12-base pair hairpin conformation with a UUCG tetra-loop for enhanced stability; no self-association or other secondary structures are formed

Steady state ATPase activity

The steady-state ATPase activity of Mss116 (50 nM) was measured at 25 °C in KMg75 buffer (75 mM KCl, 20 mM K-HEPES (pH 7.5), 5 mM $MgCl_2$, 1 mM DTT) by absorbance at 340 nm using the ATP regenerating, NADH-coupled assay [3; 51] supplemented with saturating MgATP (10 mM) while varying the [RNA], or with near-saturating RNA (2 μM) while varying the [MgATP]. The [ADP] under our conditions is ~10-30 μM (Ref [3; 51]). Where indicated, RNAse A (up to ~0.2 Kunitz mL^{-1} final) was included in the reaction mixture. The [ATP]-dependence of the steady-state rate was fitted to the hyperbolic form of the Briggs–Haldane equation since [ATP] >> [Mss116-RNA]. The [RNA]-dependence of the steady-state ATPase rate (*v*) was fitted to the quadratic form (Supplementary material A):

$$v = k_0 + (k_{cat} - k_0)\frac{H_{tot} + R_{tot} + K_{M,RNA} - \sqrt{\left(H_{tot} + R_{tot} + K_{M,RNA}\right)^2 - 4H_{tot}R_{tot}}}{2H_{tot}} \quad (10)$$

where H_{tot} is the total [Mss116], R_{tot} is the total [RNA], k_0 is the intrinsic ATPase rate in the absence of RNA, k_{cat} is the ATPase rate at saturating RNA, and $K_{M,RNA}$ is the apparent Michaelis constant for RNA stimulation. This equation assumes a 1:1 binding stoichiometry, which is confirmed in this study (presented forthcoming) using fluorescence correlation spectroscopy (FCS) and RNA stimulated Mss116 ATPase. The stoichiometry for RNA stimulated Mss116 ATPase was determined by fitting [RNA]-dependence of Mss116 steady-state ATPase under the condition [Mss116] >> $K_{M,\,RNA}$ to the numerical solutions of

the implicit bimolecular binding equation (Supplementary material B) with the stoichiometry as the unconstrained fitting parameter.

Pre-steady-state kinetic analysis

All transient kinetic measurements were made in KMg75 buffer using an Applied Photophysics SX-20 stopped flow apparatus thermostatted at 25 ±0.1 °C. The concentrations stated are final after mixing. The average of 5-8 time courses were fitted to a sum of exponentials by nonlinear least squares fitting procedure. Uncertainties are reported as standard errors in the fits unless stated otherwise.

Nucleotide (ATP and ADP) binding to Mss116 and Mss116-RNA was measured from the fluorescence enhancement associated with Förster resonance energy transfer from Mss116 (λ_{ex} = 280 nm) to bound mant-nucleotides [3; 28; 29]. Fluorescence was monitored at 90° through a 400-nm, long-pass, colored glass filter. Association kinetic traces were recorded after rapidly mixing 2 μM Mss116 in the presence or absence of 2.2 μM RNA with varying amount of mant-nucleotide under pseudo-first-order conditions, i.e. [mant-nucleotide] >> [Mss116] [3; 29]. MantADP dissociation was measured by rapid addition of excess (5 mM) unlabeled ADP to pre-equilibrated samples of 2 μM Mss116 or Mss116-RNA and 50 μM mantADP [3; 29].

Transient P_i release was measured by mixing 1 μM Mss116 or Mss116-RNA with varying [ATP] and 5μM of the fluorescently labeled mutant of phosphate binding protein (MDCC–P_iBP) as described [3]. Background P_i was removed from all solutions, syringes, and the instrument with MOP solution containing 7-methylguanosine (50-250 μM) and purine nucleoside phosphorylase (0.1-0.3 U mL^{-1}). There was approximately five-fold enhancement in the fluorescence of MDCC- P_iBP with P_i binding (λ_{ex} = 436 nm, 460-nm long-pass emission filter). The rate and equilibrium constants of P_i binding to MDCC- P_iBP under experimental conditions comparable to those used in this study are k_+ = 117 μM^{-1} s^{-1}, k_- = 24 s^{-1}, and K_d = 0.20 μM (Ref. [52]).

Measurement of oxygen isotopic exchange during ATP hydrolysis

^{18}O isotopic exchange was used to determine the reversibility of ATP hydrolysis during steady-state cycling [31; 32; 53]. Measurements were done in KMg75 buffer containing 49% [^{18}O]-H_2O supplemented with 2 mM ATP, 4 mM phosphoenolpyruvate, and 100 U mL^{-1} pyruvate kinase to regenerate ATP. Reactions were quenched with HCl and liberated P_i was isolated and analyzed for ^{18}O content [3; 31; 53].

Fluorescence Correlation Spectroscopy (FCS)

Equilibrium binding of Mss116 and RNA was assayed by FCS in KMg75 buffer with or without 10 mM ADP using an in-house assembled instrument based around an Olympus IX-71 inverted microscope [54]. Samples were measured immediately after adding to eight-well chambered coverglasses (Nunc, Rochester, NY). Equilibrium binding titrations were done with 20 nM 5′-fluorescin labeled RNA and varying [Mss116]. Mss116 labeled non-specifically at primary amines with Alexa488 succinimidyl ester (Invitrogen) was also measured.

Each final autocorrelation curve represents the average of 10 consecutive 10 second measurements. Statistical variations from the average were weighted in the curve fitting procedure. Autocorrelation curves were fitted to the following expressions for either one or two component diffusion in a three-dimensional Gaussian volume [33; 34; 35], respectively:

$$G(\tau)=\frac{1}{N}\left(1+\frac{\tau}{\tau_{\text{average}}}\right)^{-1}\left(1+\frac{s^2\tau}{\tau_{\text{average}}}\right)^{-1/2}$$

$$G(\tau)=\frac{1}{N}\left(f\left(1+\frac{\tau}{\tau_{\text{RNA}}}\right)^{-1}\left(1+\frac{s^2\tau}{\tau_{\text{RNA}}}\right)^{-1/2}+(1-f)\left(1+\frac{\tau}{\tau_{\text{complex}}}\right)^{-1}\left(1+\frac{s^2\tau}{\tau_{\text{complex}}}\right)^{-1/2}\right) \quad (11),$$

where N is the total number of molecules detected and f is the fraction of free RNA. The ratio of the radial to axial dimensions of the focal volume (s) was determined as a free parameter with Alexa488 hydrazide dye and constrained to the experimentally determined value of 0.2 during fitting. When fitting to a two component autocorrelation function [33], all time courses were fitted globally with shared RNA (τ_{RNA}) and Mss116-RNA (τ_{complex}) diffusion times. The [Mss116]-dependence of the Mss116-RNA complex was fitted to the following fractional bimolecular equilibrium binding expression:

$$\frac{[HR]}{R_{\text{tot}}}=\frac{H_{\text{tot}}+R_{\text{tot}}+K_{\text{d}}-\sqrt{(H_{\text{tot}}+R_{\text{tot}}+K_{\text{d}})^2-4H_{\text{tot}}R_{\text{tot}}}}{2R_{\text{tot}}} \quad (12),$$

where HR is Mss116-RNA and K_{d} is the RNA equilibrium binding affinity of Mss116. The [Mss116]-dependence of the RNA diffusion time (τ_{average}) from fitting to a single species autocorrelation function [33] represents the weighted average diffusion time of free RNA (τ_{RNA}) and Mss116-bound RNA (τ_{complex}) according to:

$$\tau_{\text{average}}=\frac{\tau_{\text{RNA}}[R]+\tau_{\text{complex}}[HR]}{R_{\text{tot}}}=\tau_{\text{RNA}}+\left(\tau_{\text{complex}}-\tau_{\text{RNA}}\right)\frac{[HR]}{R_{\text{tot}}} \quad (13),$$

which can be rearranged to:

$$\tau_{\text{average}}=\tau_{\text{RNA}}+\left(\tau_{\text{complex}}-\tau_{\text{RNA}}\right)\frac{H_{\text{tot}}+R_{\text{tot}}+K_{\text{d}}-\sqrt{(H_{\text{tot}}+R_{\text{tot}}+K_{\text{d}})^2-4H_{\text{tot}}R_{\text{tot}}}}{2R_{\text{tot}}} \quad (14)$$

using mass conservation and Eq. 12.

RNA duplex unwinding

An RNA duplex unwinding substrate was constructed by annealing a fluorescein-labeled 8-mer RNA fragment to a 32-mer RNA [4]. This substrate was selected because it has been thoroughly characterized in terms of its stability and unwinding by the DEAD-box protein, DbpA [4]. Duplex strand displacement was performed under single turnover conditions with [*Mss116*] >> [*dsRNA*]. RNA duplex (200 nM) equilibrated with 4 μM Mss116 was rapidly mixed with 2 mM ATP or buffer and the labeled 8-mer strand displacement was monitored from changes in fluorescence intensity and anisotropy [4].

Kinetic modeling

Kinetic simulations were performed with Tenua (available free at http://bililite.com/tenua/) or Kintek Global Kinetic Explorer (Kintek Co., Texas).

Supplementary Material

Refer to Web version on PubMed Central for supplementary material.

Acknowledgments

This work is supported by NSF-CAREER Award (MCB-0546353) to E.M.D.L.C. E.M.D.L.C. is an American Heart Association Established Investigator (0940075N) and a Hellman Family Fellow. W.C. was supported in part by American Heart Association postdoctoral fellowship award X0625997T. E.R. is supported by the Ellison Medical Foundation. E.R.M. acknowledges support from the NIH Institutional Training Grant GM08203.

References

1. Cordin O, Banroques J, Tanner NK, Linder P. The DEAD-box protein family of RNA helicases. Gene. 2006; 367:17–37. [PubMed: 16337753]
2. Pyle AM. Translocation and unwinding mechanisms of RNA and DNA helicases. Annu Rev Biophys. 2008; 37:317–36. [PubMed: 18573084]
3. Henn A, Cao W, Hackney DD, De La Cruz EM. The ATPase cycle mechanism of the DEAD-box rRNA helicase, DbpA. J Mol Biol. 2008; 377:193–205. [PubMed: 18237742]
4. Henn A, Cao W, Licciardello N, Heitkamp SE, Hackney DD, De La Cruz EM. Pathway of ATP utilization and duplex rRNA unwinding by the DEAD-box helicase, DbpA. Proc Natl Acad Sci U S A. 2010; 107:4046–50. [PubMed: 20160110]
5. Liu F, Putnam A, Jankowsky E. ATP hydrolysis is required for DEAD-box protein recycling but not for duplex unwinding. Proc Natl Acad Sci U S A. 2008; 105:20209–14. [PubMed: 19088201]
6. Chen Y, Potratz JP, Tijerina P, Del Campo M, Lambowitz AM, Russell R. DEAD-box proteins can completely separate an RNA duplex using a single ATP. Proc Natl Acad Sci U S A. 2008; 105:20203–8. [PubMed: 19088196]
7. Staley JP, Guthrie C. An RNA switch at the 5′ splice site requires ATP and the DEAD box protein Prp28p. Mol Cell. 1999; 3:55–64. [PubMed: 10024879]
8. Wassarman DA, Steitz JA. RNA splicing. Alive with DEAD proteins. Nature. 1991; 349:463–4. [PubMed: 1825133]
9. Iggo RD, Jamieson DJ, MacNeill SA, Southgate J, McPheat J, Lane DP. p68 RNA helicase: identification of a nucleolar form and cloning of related genes containing a conserved intron in yeasts. Mol Cell Biol. 1991; 11:1326–33. [PubMed: 1996094]
10. Schmid SR, Linder P. D-E-A-D protein family of putative RNA helicases. Mol Microbiol. 1992; 6:283–91. [PubMed: 1552844]
11. Rubin GM, Yandell MD, Wortman JR, Gabor Miklos GL, Nelson CR, Hariharan IK, Fortini ME, Li PW, Apweiler R, Fleischmann W, Cherry JM, Henikoff S, Skupski MP, Misra S, Ashburner M, Birney E, Boguski MS, Brody T, Brokstein P, Celniker SE, Chervitz SA, Coates D, Cravchik A, Gabrielian A, Galle RF, Gelbart WM, George RA, Goldstein LS, Gong F, Guan P, Harris NL, Hay BA, Hoskins RA, Li J, Li Z, Hynes RO, Jones SJ, Kuehl PM, Lemaitre B, Littleton JT, Morrison DK, Mungall C, O'Farrell PH, Pickeral OK, Shue C, Vosshall LB, Zhang J, Zhao Q, Zheng XH, Lewis S. Comparative genomics of the eukaryotes. Science. 2000; 287:2204–15. [PubMed: 10731134]
12. Liu ZP, Nakagawa O, Nakagawa M, Yanagisawa H, Passier R, Richardson JA, Srivastava D, Olson EN. CHAMP, a novel cardiac-specific helicase regulated by MEF2C. Dev Biol. 2001; 234:497–509. [PubMed: 11397016]
13. Rocak S, Linder P. DEAD-box proteins: the driving forces behind RNA metabolism. Nat Rev Mol Cell Biol. 2004; 5:232–41. [PubMed: 14991003]
14. Huang HR, Rowe CE, Mohr S, Jiang Y, Lambowitz AM, Perlman PS. The splicing of yeast mitochondrial group I and group II introns requires a DEAD-box protein with RNA chaperone function. Proc Natl Acad Sci U S A. 2005; 102:163–8. [PubMed: 15618406]
15. Solem A, Zingler N, Pyle AM. A DEAD protein that activates intron self-splicing without unwinding RNA. Mol Cell. 2006; 24:611–7. [PubMed: 17188036]
16. Halls C, Mohr S, Del Campo M, Yang Q, Jankowsky E, Lambowitz AM. Involvement of DEAD-box proteins in group I and group II intron splicing. Biochemical characterization of Mss116p, ATP hydrolysis-dependent and -independent mechanisms, and general RNA chaperone activity. J Mol Biol. 2007; 365:835–55. [PubMed: 17081564]

17. Seraphin B, Simon M, Boulet A, Faye G. Mitochondrial splicing requires a protein from a novel helicase family. Nature. 1989; 337:84–7. [PubMed: 2535893]
18. Bifano AL, Turk EM, Caprara MG. Structure-guided mutational analysis of a yeast DEAD-box protein involved in mitochondrial RNA splicing. J Mol Biol. 2010; 398:429–43. [PubMed: 20307546]
19. Niemer I, Schmelzer C, Borner GV. Overexpression of DEAD box protein pMSS116 promotes ATP-dependent splicing of a yeast group II intron in vitro. Nucleic Acids Res. 1995; 23:2966–72.
20. Del Campo M, Mohr S, Jiang Y, Jia H, Jankowsky E, Lambowitz AM. Unwinding by local strand separation is critical for the function of DEAD-box proteins as RNA chaperones. J Mol Biol. 2009; 389:674–93. [PubMed: 19393667]
21. Del Campo M, Tijerina P, Bhaskaran H, Mohr S, Yang Q, Jankowsky E, Russell R, Lambowitz AM. Do DEAD-box proteins promote group II intron splicing without unwinding RNA? Mol Cell. 2007; 28:159–66. [PubMed: 17936712]
22. Zingler N, Solem A, Pyle AM. Dual roles for the Mss116 cofactor during splicing of the ai5gamma group II intron. Nucleic Acids Res. 2010; 38:6602–9. [PubMed: 20554854]
23. Karunatilaka KS, Solem A, Pyle AM, Rueda D. Single-molecule analysis of Mss116-mediated group II intron folding. Nature. 2010; 467:935–9. [PubMed: 20944626]
24. Mohr G, Del Campo M, Mohr S, Yang Q, Jia H, Jankowsky E, Lambowitz AM. Function of the C-terminal domain of the DEAD-box protein Mss116p analyzed in vivo and in vitro. J Mol Biol. 2008; 375:1344–64. [PubMed: 18096186]
25. Hannemann DE, Cao W, Olivares AO, Robblee JP, De La Cruz EM. Magnesium, ADP, and actin binding linkage of myosin V: evidence for multiple myosin V-ADP and actomyosin V-ADP states. Biochemistry. 2005; 44:8826–40. [PubMed: 15952789]
26. Robblee JP, Cao W, Henn A, Hannemann DE, De La Cruz EM. Thermodynamics of nucleotide binding to actomyosin V and VI: a positive heat capacity change accompanies strong ADP binding. Biochemistry. 2005; 44:10238–49. [PubMed: 16042401]
27. De La Cruz EM, Ostap EM. Kinetic and equilibrium analysis of the myosin ATPase. Methods Enzymol. 2009; 455:157–92. [PubMed: 19289206]
28. Moore KJ, Lohman TM. Kinetic mechanism of adenine nucleotide binding to and hydrolysis by the Escherichia coli Rep monomer. 1. Use of fluorescent nucleotide analogues. Biochemistry. 1994; 33:14550–64. [PubMed: 7981217]
29. Talavera MA, De La Cruz EM. Equilibrium and kinetic analysis of nucleotide binding to the DEAD-box RNA helicase DbpA. Biochemistry. 2005; 44:959–70. [PubMed: 15654752]
30. Chin HF, Cai Y, Menon S, Ferro-Novick S, Reinisch KM, De La Cruz EM. Kinetic analysis of the guanine nucleotide exchange activity of TRAPP, a multimeric Ypt1p exchange factor. J Mol Biol. 2009; 389:275–88. [PubMed: 19361519]
31. Hackney DD. The tethered motor domain of a kinesin-microtubule complex catalyzes reversible synthesis of bound ATP. Proc Natl Acad Sci U S A. 2005; 102:18338–43. [PubMed: 16339908]
32. Hackney DD, Stempel KE, Boyer PD. Oxygen-18 probes of enzymic reactions of phosphate compounds. Methods Enzymol. 1980; 64:60–83. [PubMed: 7374458]
33. Rhoades E, Ramlall TF, Webb WW, Eliezer D. Quantification of alpha-synuclein binding to lipid vesicles using fluorescence correlation spectroscopy. Biophys J. 2006; 90:4692–700. [PubMed: 16581836]
34. Thompson, NL. Fluorescence Correlation Spectroscopy. In: Lakowicz, JR., editor. Topics in Fluorescence Microscopy. Plenum Press; New York: 1991. p. 337-378.
35. Rigler R, Mets Ü, Widengren J, Kask P. Fluorescence correlation spectroscopy with high count rate and low background: analysis of translational diffusion. Eur. Biophys. J. 1993; 22:169–175.
36. Sheldon JG, Williams SP, Fulton AM, Brindle KM. 31P NMR magnetization transfer study of the control of ATP turnover in Saccharomyces cerevisiae. Proc Natl Acad Sci U S A. 1996; 93:6399–404. [PubMed: 8692826]
37. Aregger R, Klostermeier D. The DEAD box helicase YxiN maintains a closed conformation during ATP hydrolysis. Biochemistry. 2009; 48:10679–81. [PubMed: 19839642]

38. Theissen B, Karow AR, Kohler J, Gubaev A, Klostermeier D. Cooperative binding of ATP and RNA induces a closed conformation in a DEAD box RNA helicase. Proc Natl Acad Sci U S A. 2008; 105:548–53. [PubMed: 18184816]
39. Appleby TC, Anderson R, Fedorova O, Pyle AM, Wang R, Liu X, Brendza KM, Somoza JR. Visualizing ATP-dependent RNA translocation by the NS3 helicase from HCV. J Mol Biol. 2011; 405:1139–53. [PubMed: 21145896]
40. Jarmoskaite I, Russell R. DEAD-box proteins as RNA helicases and chaperones. WIREs RNA. 2011; 2:135–152. [PubMed: 21297876]
41. Fedorova O, Solem A, Pyle AM. Protein-facilitated folding of group II intron ribozymes. J Mol Biol. 2010; 397:799–813. [PubMed: 20138894]
42. Bifano AL, Caprara MG. A DExH/D-box protein coordinates the two steps of splicing in a group I intron. J Mol Biol. 2008; 383:667–82. [PubMed: 18789947]
43. Pan C, Russell R. Roles of DEAD-box proteins in RNA and RNP Folding. RNA Biol. 2010; 7:28–37. [PubMed: 20023408]
44. Lorsch JR, Herschlag D. The DEAD box protein eIF4A. 2. A cycle of nucleotide and RNA-dependent conformational changes. Biochemistry. 1998; 37:2194–206. [PubMed: 9485365]
45. Lorsch JR, Herschlag D. The DEAD box protein eIF4A. 1. A minimal kinetic and thermodynamic framework reveals coupled binding of RNA and nucleotide. Biochemistry. 1998; 37:2180–93. [PubMed: 9485364]
46. Polach KJ, Uhlenbeck OC. Cooperative binding of ATP and RNA substrates to the DEAD/H protein DbpA. Biochemistry. 2002; 41:3693–702. [PubMed: 11888286]
47. Sharpe Elles LM, Sykes MT, Williamson JR, Uhlenbeck OC. A dominant negative mutant of the E. coli RNA helicase DbpA blocks assembly of the 50S ribosomal subunit. Nucleic Acids Res. 2009; 37:6503–14. [PubMed: 19734347]
48. Fuller-Pace FV, Nicol SM, Reid AD, Lane DP. DbpA: a DEAD box protein specifically activated by 23s rRNA. EMBO J. 1993; 12:3619–26. [PubMed: 8253085]
49. Cole C, Barber JD, Barton GJ. The Jpred 3 secondary structure prediction server. Nucleic Acids Res. 2008; 36:W197–201. [PubMed: 18463136]
50. Del Campo M, Lambowitz AM. Structure of the Yeast DEAD box protein Mss116p reveals two wedges that crimp RNA. Mol Cell. 2009; 35:598–609. [PubMed: 19748356]
51. De La Cruz EM, Sweeney HL, Ostap EM. ADP inhibition of myosin V ATPase activity. Biophys J. 2000; 79:1524–9. [PubMed: 10969013]
52. Henn A, De La Cruz EM. Vertebrate myosin VIIb is a high duty ratio motor adapted for generating and maintaining tension. J Biol Chem. 2005; 280:39665–76. [PubMed: 16186105]
53. Olivares AO, Chang W, Mooseker MS, Hackney DD, De La Cruz EM. The tail domain of myosin Va modulates actin binding to one head. J Biol Chem. 2006; 281:31326–36. [PubMed: 16921171]
54. Elbaum-Garfinkle S, Ramlall T, Rhoades E. The role of the lipid bilayer in tau aggregation. Biophys J. 2010; 98:2722–30. [PubMed: 20513417]

- We measured the rate and equilibrium constants underlying Mss116 ATP utilization and nucleotide-linked RNA binding.
- RNA accelerates the Mss116 steady-state ATPase ~7-fold by promoting rate-limiting ATP hydrolysis, such that P_i release becomes (partially) rate-limiting.
- RNA binding displays strong thermodynamic coupling to the Mss116 nucleotide states such that Mss116 with bound ADP-P_i binds RNA much more strongly than other nucleotide states
- The predominant biochemical intermediate populated during *in vivo* steady-state cycling is the strong RNA binding, Mss116-ADP-P_i state.
- The data collectively favor a model in which ATP hydrolysis promotes a weak-to-strong RNA binding transition that disrupts stable RNA duplexes. The subsequent strong-to-weak RNA binding transition associated with P_i release dissociates RNA-Mss116 complexes, regenerating free Mss116.

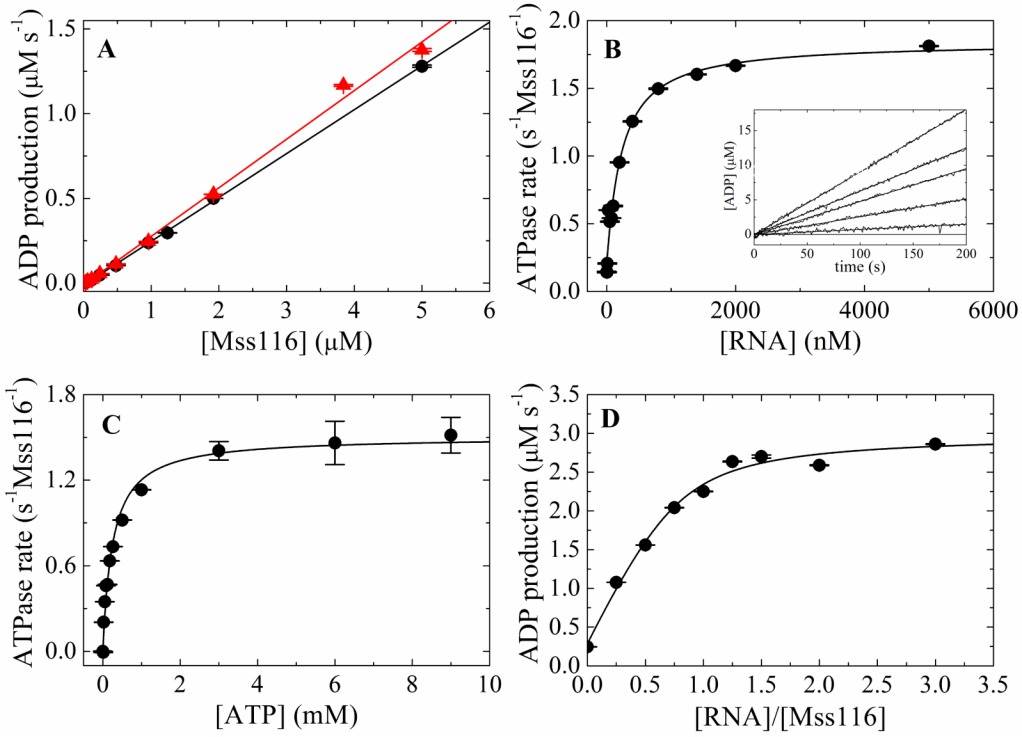

Figure 1. Steady-state ATPase activity of Mss116

A. [Mss116]-dependence of intrinsic ATPase activity in the absence of RNA and presence of 10 mM MgATP with (filled triangles, red) and without (filled circle, black) RNase A. The slope yields a k_{cat} of 0.26 s^{-1} $Mss116^{-1}$ without RNase A and 0.29 s^{-1} $Mss116^{-1}$ with RNase A. B. [RNA]-dependence of Mss116 steady-state ATPase rate in the presence of 10 mM MgATP. The solid line is the best fit to Eq. 10. The inset shows the time courses of steady state ADP production upon addition of 10 mM MgATP to a pre-equilibrated sample of 50 nM Mss116 and (lower to upper) 0, 50, 200, 400, 5000 nM RNA. The smooth lines represent the best fits to a line. C. [ATP]-dependence of Mss116 steady-state ATPase rate in the presence of 2 μM RNA. The k_{cat}, and $K_{M,ATP}$ values obtained from the best fits to the hyperbolic form of the Briggs–Haldane (solid line) are listed in Table 1. D. [RNA]-dependence of Mss116 steady-state ATPase rate measured with 2 μM (>>$K_{M,RNA}$) Mss116 in the presence of 2.4 mM MgATP for stoichiometry determination. The solid line is the best fit of the data to the implicit bimolecular binding equation (Supplementary material B) with the stoichiometry unconstrained during the fitting.

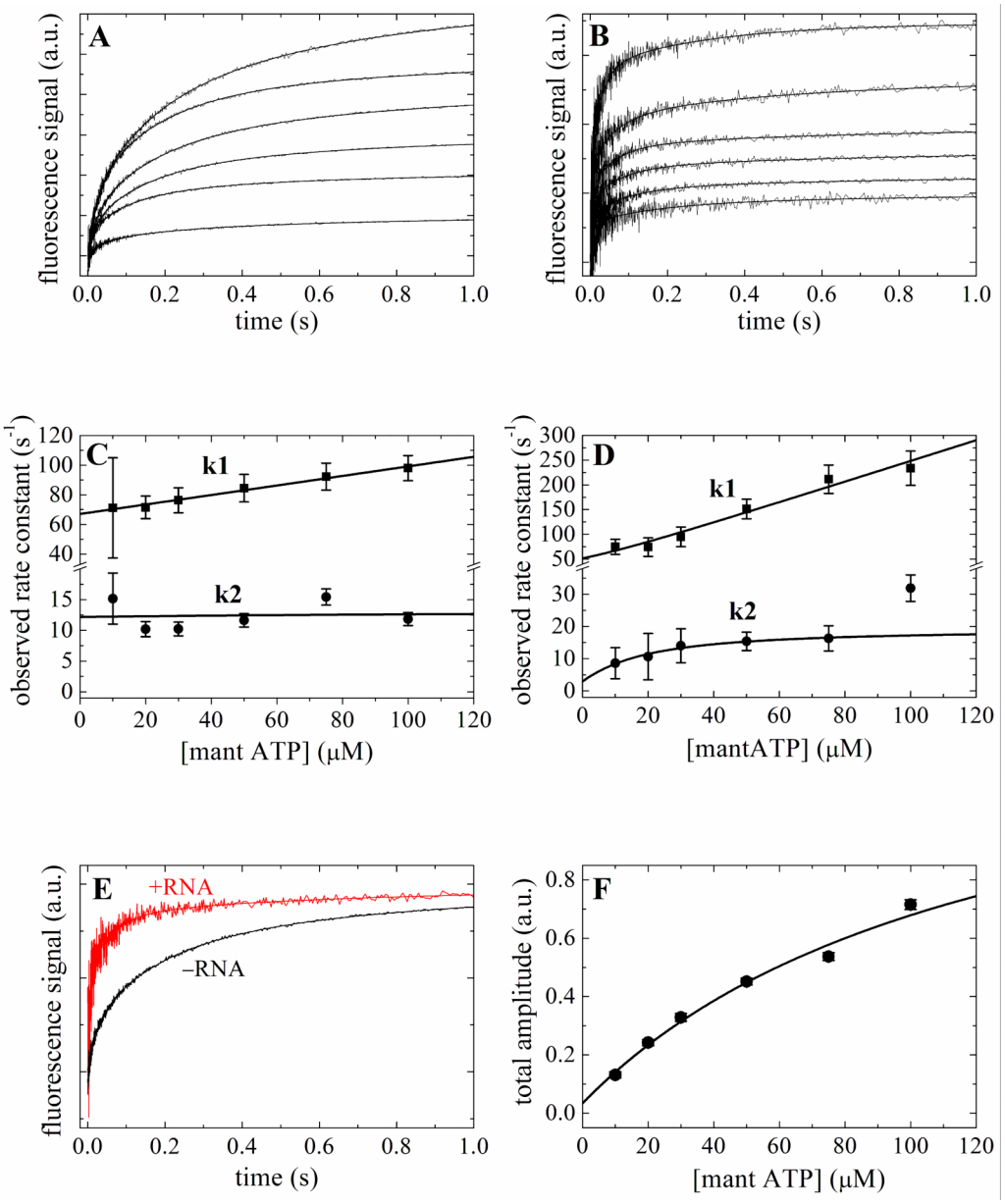

Figure 2. Kinetics of mantATP binding to Mss116 and Mss116-RNA

Time courses of fluorescence change after mixing a range of [mantATP] with 2 μM Mss116 (Panel A) or Mss116–RNA (Panel B). The smooth lines through the data are the best fits to a sum of exponentials. [mantATP]-dependence of the observed rate constants of mantATP binding to Mss116 (Panel C) or Mss116-RNA (Panel D). The solid line through the data represents the best fit to Eq. 1 [3]. E. Comparison of the time courses of 50 μM mantATP binding to Mss116 and Mss116-RNA. F. The [mantATP]-dependence of the total fluorescence change amplitude associated with mantATP binding to Mss116. The solid line is the best fit to a hyperbola, for which the $K_{0.5}$ presents the overall mantATP-Mss116 equilibrium binding constant.

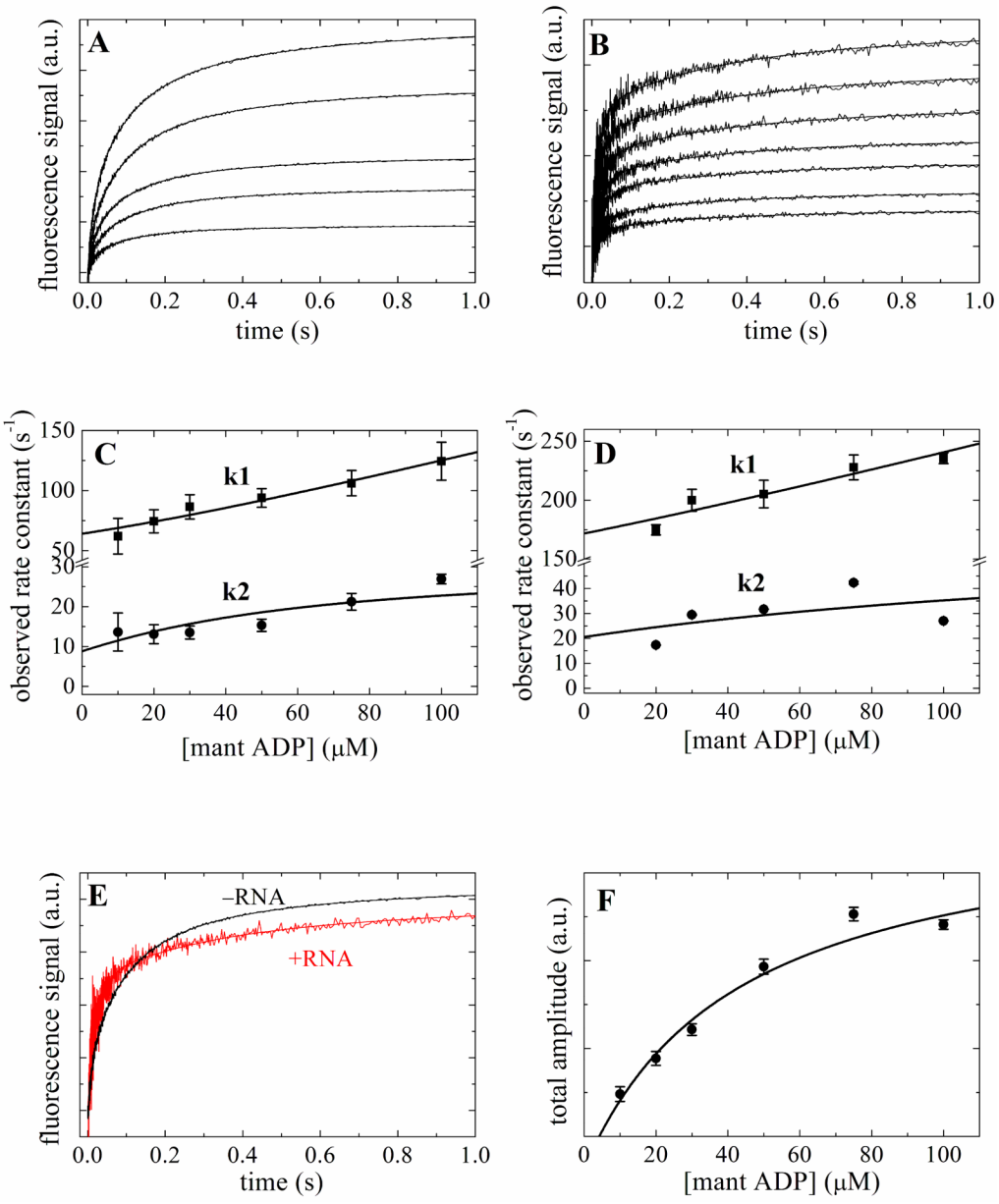

Figure 3. Kinetics of mantADP binding to Mss116 and Mss116-RNA

Time courses of fluorescence change after mixing a range of [mantADP] with 2 μM Mss116 (Panel A) or Mss116–RNA (Panel B). The smooth lines through the data are the best fits to a sum of exponentials. [mantADP]-dependence of the observed rate constants of mantADP binding to Mss116 (Panel C) or Mss116-RNA (Panel D). The solid line through the data represents the best fit to quadratic equations Eq. 4 [3; 25] for two-step binding. E. Comparison of the time courses of 50 μM mantADP binding to Mss116 and Mss116-RNA. F. The [mantATP]-dependence of the total fluorescence change amplitude associated with mantATP binding to Mss116. The solid line is the best fit to a hyperbola, for which the $K_{0.5}$ presents the overall mantADP-Mss116 equilibrium binding constant.

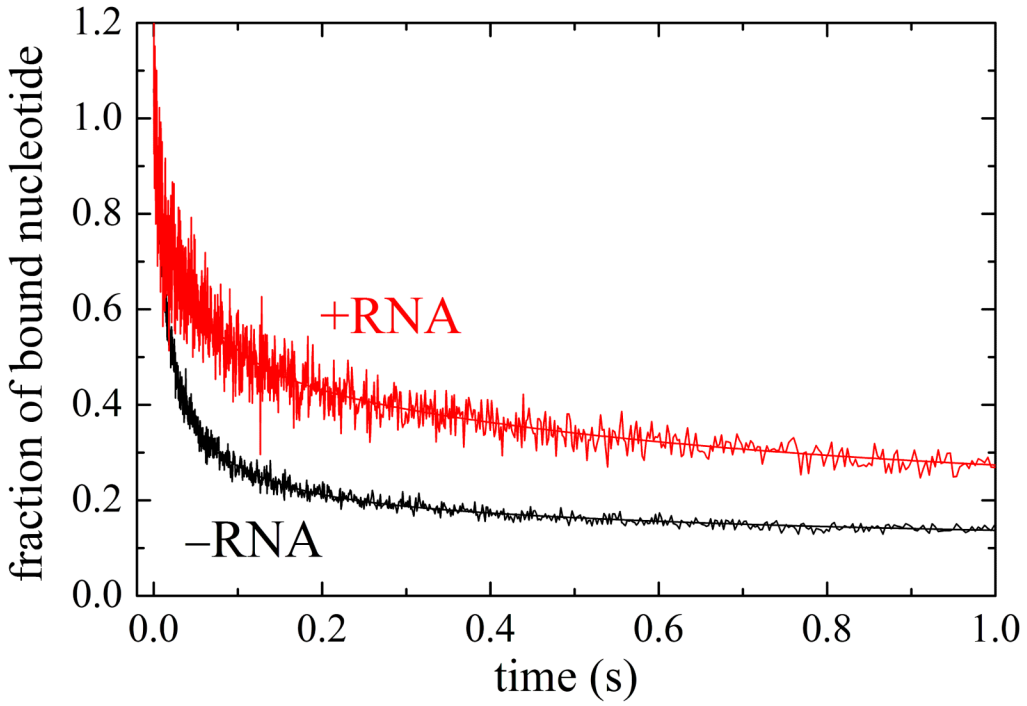

Figure 4. Kinetics of mantADP dissociation from Mss116 with and without RNA

Time courses of irreversible mantADP dissociation from Mss116 and Mss116-RNA after mixing 2 mM ADP with 2 μM Mss116 or Mss116-RNA pre-equilibrated with 50 μM mantADP. The smooth lines through the data are the best fits to a sum of exponentials.

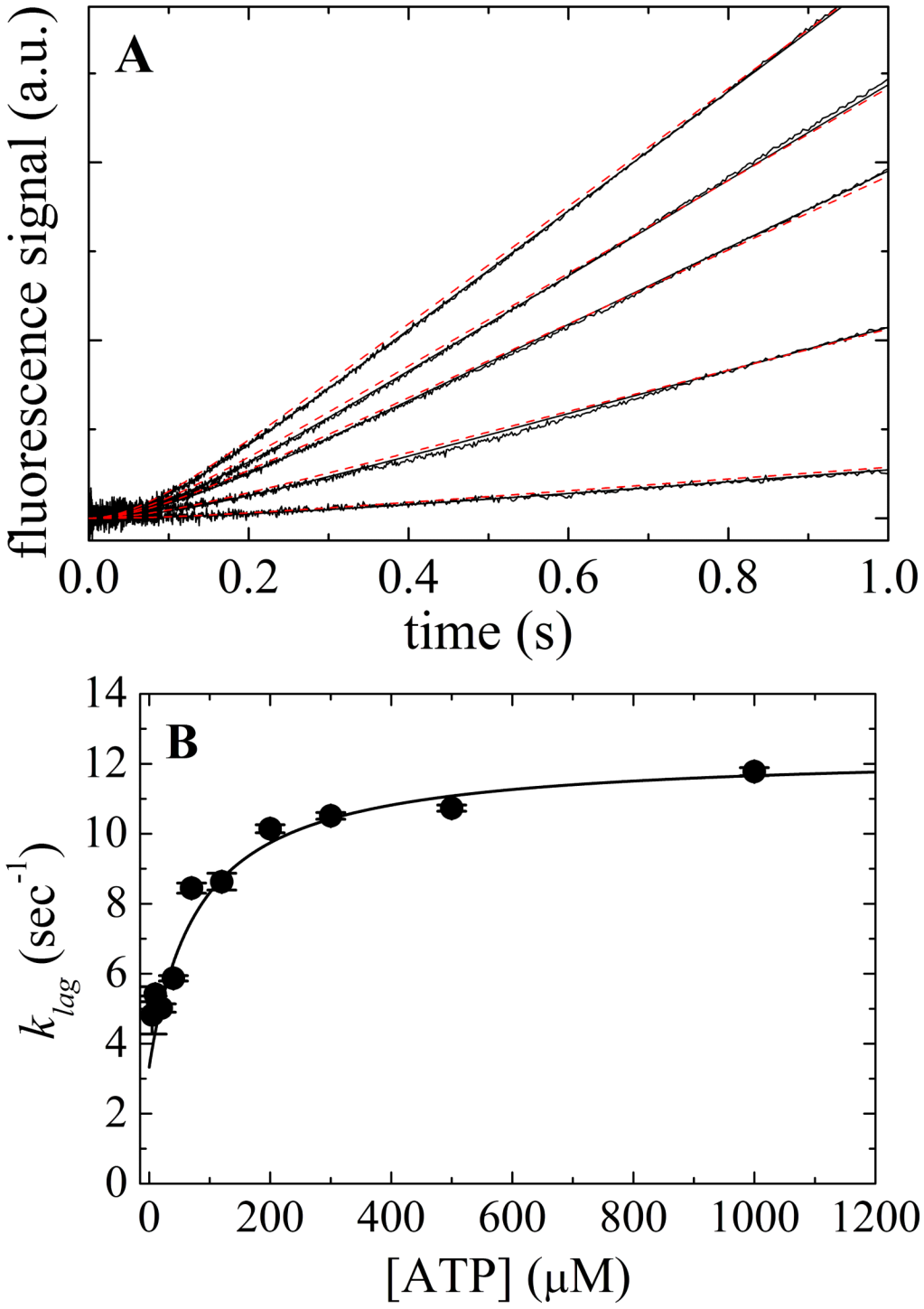

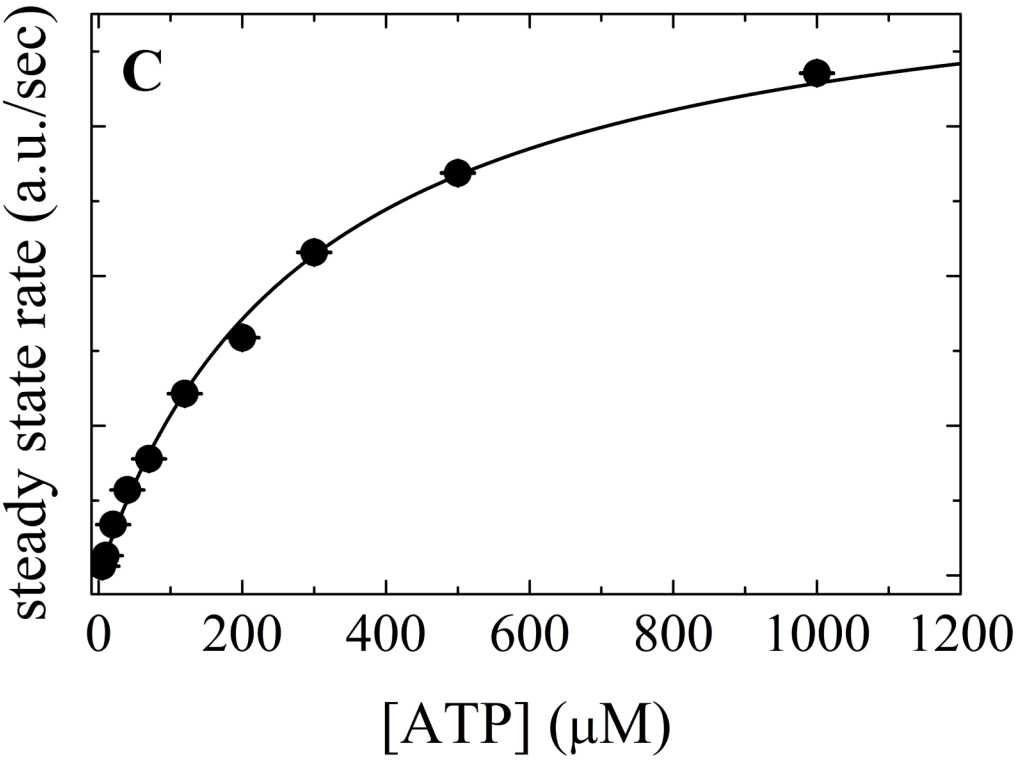

Figure 5. Kinetics of transient P_i release from ATP hydrolysis by Mss116-RNA

A. Time courses of P_i release from ATP hydrolysis by Mss116-RNA (pre-equilibrated sample of 1 μM Mss116 and 2 μM RNA) after mixing with 20, 120, 300, 500 and 1000 μM MgATP (lower to upper). The smooth lines through the data are the best fits to the phosphate release equation (Eq. 7) and the red dotted lines represent simulated time courses using Scheme 1 and the rate and equilibrium constants tabulated in Table 1. B. [ATP]-dependence of the observed lag phase rate constant. The smooth line is the best fit to a hyperbola. C. [ATP]-dependence of the steady-state rate obtained from the linear regime of time courses. The solid line through the data represents the best fit to a hyperbola, yielding obtained $K_{M,ATP}$ of 300 μM (Table 1).

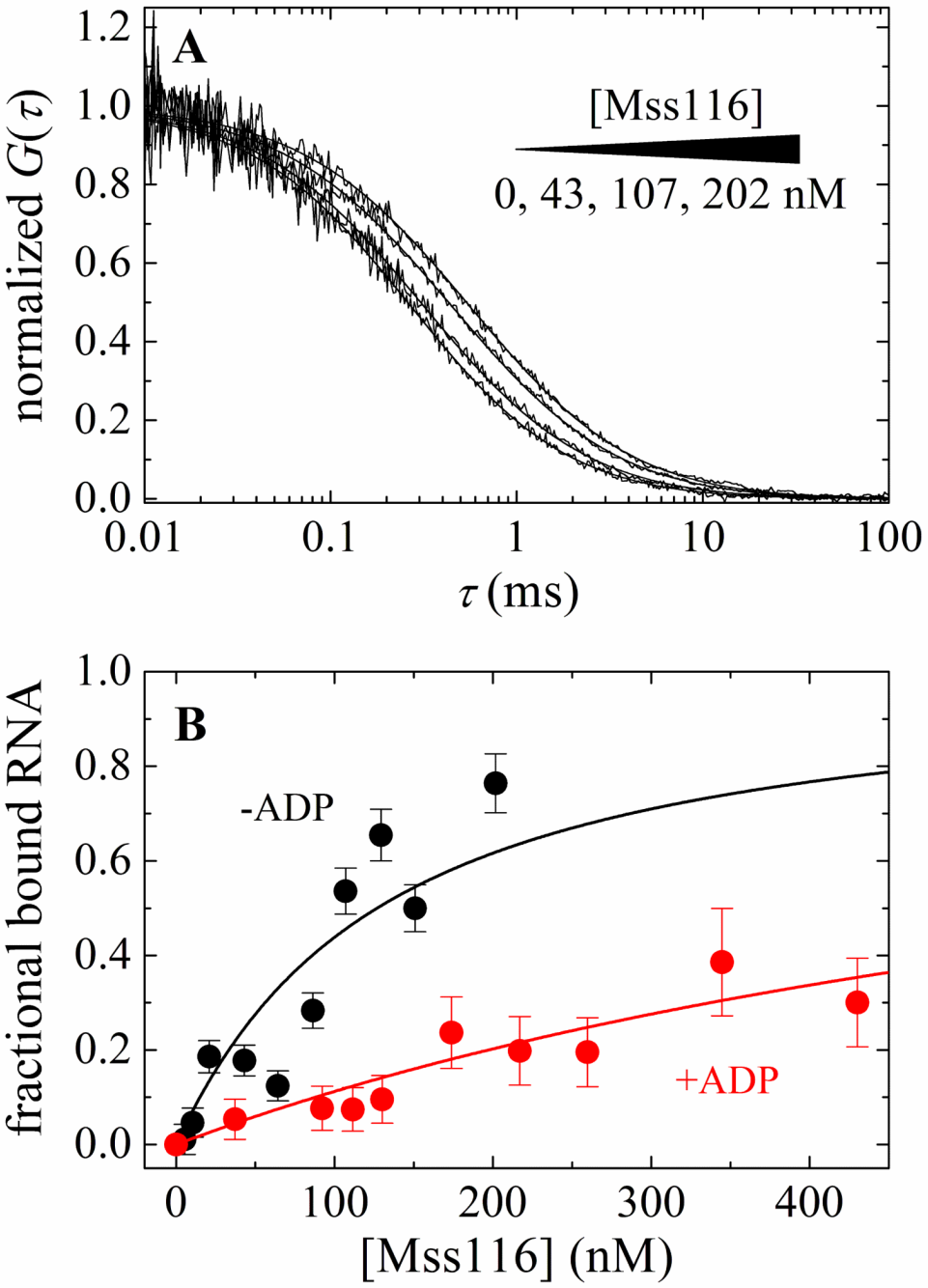

Figure 6. FCS measurements of equilibrium RNA binding to Mss116 and Mss116-ADP

A. Normalized autocorrelation curves of 20 nM fluorescein-labeled RNA in the presence of (from left to right) 0, 43, 107, or 202 nM Mss116. The smooth lines though the data represent a global fit to a two-species autocorrelation function (Eq. 11). B. [Mss116]- and [Mss116-ADP]-dependence of the fraction of total bound RNA obtained from global fit of autocorrelation curves of different Mss116 concentration to standard two-species autocorrelation function. The solid line through the data represents the best fit to the quadratic function for equilibrium bimolecular binding (Eq. 12) with the maximum value constrained to unity. The nucleotide-dependent RNA binding affinities are summarized in

Table 1. Analysis of the average diffusion time ($\tau_{average}$) yielded comparable results (Table 1).

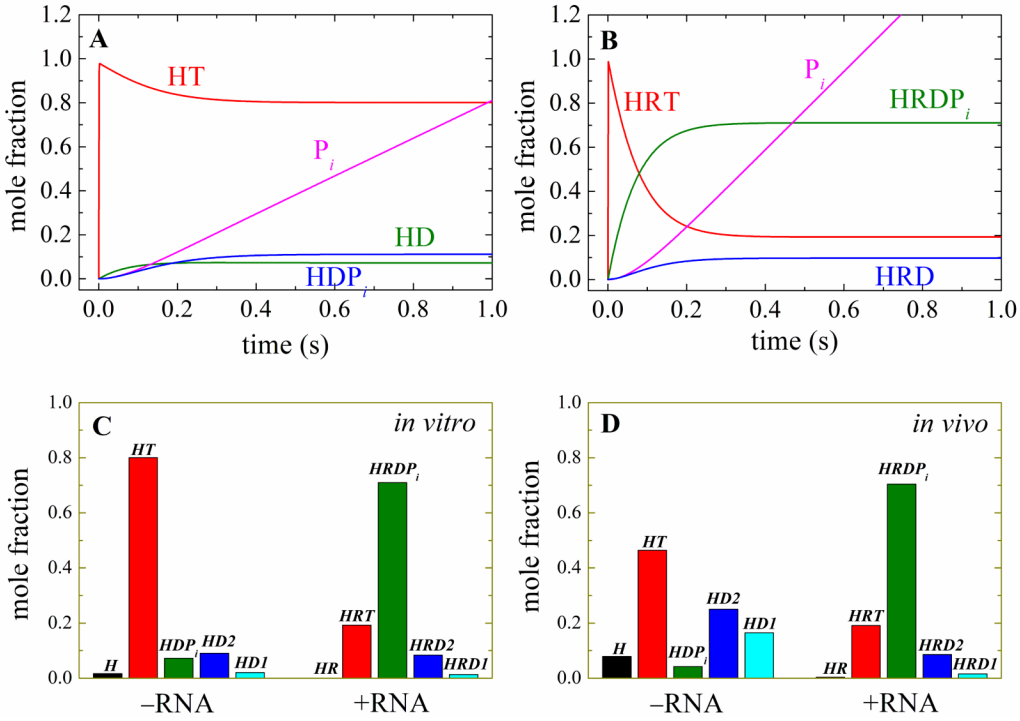

Figure 7. Population and steady-state distribution of ATPase cycle biochemical intermediates

Simulated time courses of the Mss116 (Panel A) or Mss116-RNA (Panel B) populated biochemical intermediate mole fraction upon addition of 10 mM ATP and 30 μM ADP (*in vitro* nucleotide concentrations). C. Steady state distribution of ATPase cycle intermediates under *in vitro* conditions. D. Steady state distribution of ATPase cycle intermediates under *Saccharomyces cerevisiae* mitochondria *in vivo* nucleotide concentrations (1.2 mM ATP, 0.11 mM ADP and 2.7 mM P_i when grown in the presence of 110 mM glucose [36]).

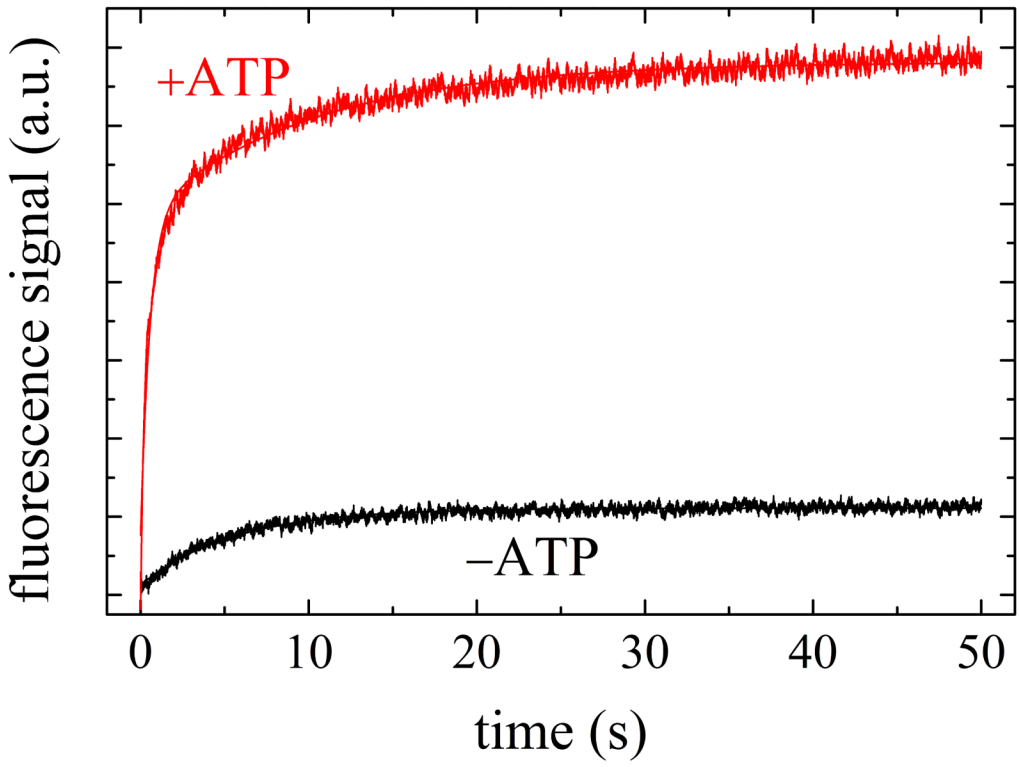

Figure 8. RNA duplex unwinding by Mss116

Time courses of RNA duplex unwinding after mixing a pre-equilibrated sample of 4 μM Mss116 and 200 nM duplex RNA with 2 mM ATP (red) or buffer (black). The smooth line through the data with ATP is the best fit to a double exponential, while the smooth line through the data acquired in the absence of ATP is the best fit to a single exponential.

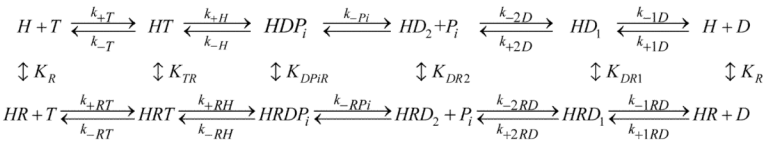

Scheme 1.

Table 1

Rate and equilibrium[a] constants of the Mss116 ATPase cycle

Steady-state parameters		
k_{cat} (−RNA)	0.26 (± 0.002) s^{-1}Mss116^{-1}′	(ATPase without RNase, Fig. 1A)
	0.29 (± 0.006) s^{-1}Mss116^{-1}	(ATPase with RNase, Fig. 1A)
	0.20 (± 0.05) s^{-1}Mss116^{-1}	(NADH assay, y-intercept, Fig. 1B)
	0.77 s^{-1}Mss116^{-1}	(predicted by Eq. A24 & mantATP)
k_{cat} (+RNA)	1.8 (± 0.07) s^{-1}Mss116^{-1}	(NADH assay, Fig. 1B)
	1.5 (± 0.4) s^{-1} Mss116^{-1}	(NADH assay, Fig. 1C)
	1.7 s^{-1}Mss116^{-1}	(predicted by Eq. A23 & P_i release)
	2.1 s^{-1} Mss116^{-1}	(predicted by Eq. A23 & mantATP)
$K_{M,ATP}$ (−RNA)	288 μM	(predicted by Eq. 42 in ref.[3] & mantATP)
$K_{M,ATP}$ (+RNA)	252 (± 27) μM	(NADH assay, Fig. 1C)
	299 (± 0.3) μM	(P_i release, K_M of steady state, Fig. 6C)
	24.5 μM	(predicted by Eq. 42 in ref.[3] & P_i release)
	19.8 μM	(predicted by Eq. 42 in ref.[3] & mantATP)
$K_{M,RNA}$	205 (± 45) nM	(NADH assay, Fig. 1B)
	74 nM	(predicted by Eq. A21 & P_i release)
	84 nM	(predicted by Eq. A21 & mantATP)
Stoichiometry	0.9 (±0.1) RNA/Mss116	(ATPase at [Mss] >> $K_{M,RNA}$; Fig. 1D)
ATP binding		
k_{+1T}	0.33 (± 0.04) μM^{-1} s^{-1}	(mantATP, Fig. 2C)
k_{-1T}	66 (± 8) s^{-1}	(mantATP, Fig. 2C)
K_{1T}	200 (± 34) μM	(mantATP, ratio of rate const., Fig. 2C)
$K_{T,overall}$	126 (± 35) μM	(mantATP total fluor. change, Fig. 2E)
k_{+RT}	2.1 (± 0.2) μM^{-1} s^{-1}	(mantATP, Fig. 2D)
k_{-RT}	35 (± 7) s^{-1}	(mantATP, Fig. 2D)
K_{RT}	17 (± 4) μM	(mantATP ratio of rate const., Fig. 2D)
	80 (± 7) μM	(P_i release, $K_{0.5}$ of lag, Fig. 5B)
Hydrolysis & P_i release		
P_c(−RNA)	0.147 (± 0.004)	(^{18}O Exchange)
$\lambda_{slow,\infty}$	13.3 (± 6) s^{-1}	(mantATP slow rate maximum, Fig. 2C)
$\lambda_{slow,0}$	12.4 (± 1) s^{-1}	(mantATP slow rate intercept, Fig. 2C)
k_{+H}	1.1 s^{-1}	(^{18}O Exchange & mantATP, Fig. 2C)
k_{-H}	1.8 s^{-1}	(^{18}O Exchange & mantATP, Fig. 2C)
$K_H = k_{-H}/k_{+H}$	1.7	(^{18}O Exchange & mantATP, Fig. 2C)
k_{-Pi}	10.4 s^{-1}	(^{18}O Exchange & mantATP, Fig. 2C)
P_c(+RNA)	0.088 (± 0.003)	(^{18}O Exchange)
$\lambda_{lag,\infty}$	12.3 (± 0.3) s^{-1}	(P_i release, Fig. 5B)

	19.5 (± 1) s^{-1}	(mantATP slow rate maximum, Fig. 2D)
$\lambda_{lag,0}$	3.3 (± 0.2) s^{-1}	(P_i release, Fig. 5B)
	4.3 (± 1) s^{-1}	(mantATP slow rate intercept, Fig. 2D)
k_{+RH}	9.7 s^{-1}	(^{18}O Exchange & P_i release)
	16.5 s^{-1}	(^{18}O Exchange & mantATP, Fig. 2D)
k_{-RH}	0.23s^{-1}	(^{18}O Exchange & P_i release)
	0.26 s^{-1}	(^{18}O Exchange & mantATP, Fig. 2D)
$K_{RH} = k_{-RH}/k_{+RH}$	0.024	(^{18}O Exchange & P_i release)
	0.016	(^{18}O Exchange & mantATP, Fig. 2D)
k_{-RPi}	2.4 s^{-1}	(^{18}O Exchange & P_i release)
	2.7 s^{-1}	(^{18}O Exchange & mantATP, Fig. 2D)
ADP binding		
k_{+1D}	0.75 (±0.07) μM^{-1} s^{-1}	(mantADP, Fig. 3C)
k_{-1D}	42 (±7) s^{-1}	(mantADP, Fig. 3C)
K_{1D}	56 (± 11) μM	(mantADP, ratio of rate const., Fig. 3C)
k_{+2D}	17 (± 8) s^{-1}	(mantADP, Fig. 3C)
k_{-2D}	13 (± 4) s^{-1}	(mantADP, Fig. 3C)
K_{2D}	0.77 (± 0.4)	(mantADP ratio of rate const.,Fig. 3C)
$K_{D, overall}$	43 (± 12) μM	(mantADP binding amplitude, Fig. 3E)
	25 μM	(overall binding, Eq. 3 in ref. [3])
$k_{D,diss1}$	69.2 (± 3) s^{-1}	(mantADP dissociation, Fig. 4)
	64.1 s^{-1}	(predicted by Eq. 5)
$k_{D,diss2}$	13.2 (± 1) s^{-1}	(mantADP dissociation, Fig. 4)
	8.8 s^{-1}	(predicted by Eq. 5)
k_{+1RD}	0.84 (± 0.2) μM^{-1} s^{-1}	(mantADP, Fig. 3D)
k_{-1RD}	133 (± 32) s^{-1}	(mantADP, Fig. 3D)
K_{1RD}	158 (± 54) μM	(mantADP ratio of rate const., Fig. 3D)
k_{+2RD}	32.7 (± 30) s^{-1}	(mantADP, Fig. 3D)
k_{-2RD}	26.5 (± 7) s^{-1}	(mantADP, Fig. 3D)
K_{2RD}	0.81 (± 0.7)	(mantADP ratio of rate const., Fig. 3D)
$K_{RD,overall}$	91.6 (± 8) μM	(mantADP binding total amplitude)
	70.9 μM	(overall binding, Eq. 3 in ref. [3])
$k_{RD,diss1}$	194.0 (± 51) s^{-1}	(mantADP dissociation, Fig.4)
	172 s^{-1}	(predicted by Eq. 5)
$k_{RD,diss2}$	16.9 (± 2) s^{-1}	(mantADP dissociation, Fig.4)
	20.5 s^{-1}	(predicted by Eq. 5)
3-D diffusion		
τ_{RNA}	0.27 (± 0.008) ms	(FCS, global fit with 2 species, Fig. 6A)
$\tau_{RNA, ADP}$	0.26 (± 0.008) ms	(FCS, global fit with 2 species)
$\tau_{Mss116-RNA}$	0.69 (± 0.04) ms	(FCS, global fit with 2 species, Fig. 6A)

$\tau_{Mss116\text{-}ADP\text{-}RNA}$	0.56 (± 0.08) ms	(FCS, global fit with 2 species)
τ_{Mss116}	0.52 ms	(FCS, , fit 1 species)
duplex RNA strand displacement		
k_{sd} (+ATP)	2.1 (±0.01) s^{-1}	(unwinding, fast phase with ATP, Fig. 8)
k_{sd} (−ATP)	0.11 (±0.0004) s^{-1}	(unwinding, slow phase with ATP, Fig 8)
	0.18 (±0.0009) s^{-1}	(unwinding without ATP, Fig. 8)
RNA binding		
K_R	117 (± 21) nM	(FCS, fractional complex fit, Fig. 6B)
	122 (± 22) nM	(FCS, average diffusing time fit,)
K_{TR}	47 nM	(calculated from detailed balance) [b]
K_{DPiR}	2 nM	(calculated from detailed balance) [c]
K_{DR1}	328 nM	(calculated from detailed balance) [d]
K_{DR2}	345 nM	(calculated from detailed balance) [e]
$K_{DR,\ overall}$	775 (± 316) nM	(FCS, fractional complex fit, Fig. 6B)
	848 (± 91) nM	(FCS, average diffusing time fit,)
	336 nM	(calculated from detailed balance) [f]

[a] $K_i = k_{-i}/k_{+i}$ represent dissociation equilibrium constants.

[b] Calculated from $K_{TR} = K_{RT}\, K_R/K_T$.

[c] Calculated from $K_{DPiR} = K_{RH}\, K_{TR}/K_H$.

[d] Calculated from $K_{1DR} = K_{1RD}\, K_R/K_{1D}$.

[e] Calculated from $K_{2DR} = K_{2RD}\, K_{1DR}/K_{2D}$.

[f] Calculated from $K_{DR,overall} = K_{RD,overall}\, K_R/K_{D,overall}$.